Nanoscale

Accepted Manuscript

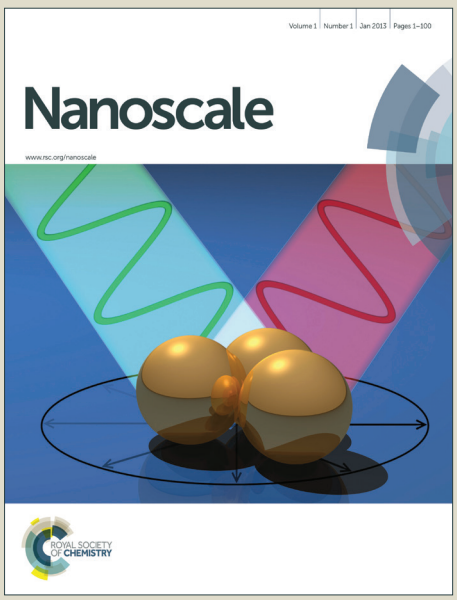

ROYAL SOCIETY OF CHEMISTRY

www.rsc.org/nanoscale

Journal Name ARTICLE

Improving the Efficiency of Polymer Solar Cells Based on Furan-Flanked Diketopyrrolopyrrole Copolymer via Solvent Additive and Methanol Treatment

Received 00th January 20xx,
Accepted 00th January 20xx

DOI: 10.1039/x0xx00000x

www.rsc.org/

Weilong Zhou,[a] Huajie Chen,[b] Junjie Lv,[a] Youchun Chen,[a] Weifeng Zhang,[b*] Gui Yu[b*] and Fenghong Li[a]*

We present a furan-flanked DPP copolymer poly{3,6-difuran-2-yl-2,5-di(2-octyldodecyl)-pyrrolo [3,4-c]pyrrole-1,4-dione-altthienylenevinylene} (PDVF-8) and highlight improving the power conversion efficiency (PCE) of polymer solar cells (PSCs) based on the PDVF-8 as an electron donor via solvent additive and methanol treatment. When 3 vol% 1, 8-diiodooctane (DIO) or 1-chloronaphthalene (CN) was used as a solvent additive of PDVF-8:$PC_{71}BM$ solution in chloroform (CF), the PCE can increase from 0.79% to 3.73% or 4.26%. Methanol treatment (MT) can further enhance the PCE to 4.03% (DIO) and 4.69% (CN), respectively. Effect of solvent additives (DIO and CN) and MT on the phase separation of the PDVF-8:$PC_{71}BM$ thin film has been investigated using atomic force microscopy, transmission electron microscopy (TEM), TEM-energy dispersive spectroscopy and x-ray photoemission spectroscopy depth profiling in details.

1. Introduction

Polymer solar cells (PSCs) have drawn great attention owing to their key advantages of synthetic variability, light weight, low cost, large-area roll to roll fabrication and the lucrative possibility of integration directly into flexible devices.[1-5] Currently photoactive layer of the most efficient PSCs is a bulk blend composed of an electron-accepting fullerene derivative and an electron-donating conjugated polymer (CP).[6-10] In order to optimize the overall performance of the PSCs, the CPs should have a narrow band gap for efficient solar energy harvesting,[11] a low-lying highest occupied molecular orbital (HOMO) to maximize the open circuit voltage (Voc),[12] and a lowest unoccupied molecular orbital (LUMO) level that is appropriately offset above the acceptor's LUMO to drive charge separation while minimizing energy loss.[13] In addition, charge carrier mobility and morphology of the active layer are also crucial elements limiting the efficiency of the PSCs.[14, 15] Recently the synthesis of the CPs by alternating electron-rich and electron-poor moieties along the backbone has emerged as an effective way to tune the optical and electronic properties of the CPs.[15, 16] Diketopyrrolopyrrole (DPP) is one of the successful electron deficient units used in the CPs as an electron donor of the PSCs.[12, 15-28] The strong electron deficient character of DPP allows synthesizing materials that absorb in the near infrared and shows ambipolar charge transport in organic field effect transistors with good mobilities for holes and electrons.[29-32] 5-membered rings are preferred for the substitutions at the 3- and 6-positions of DPP unit because they alleviate steric hindrance and extend the effective conjugation length through increased coplanarity. Substitution of the thiophene with furan flanking the DPP core was firstly reported in 2010 by Fréchet et al.[20] Inserting furan moieties in the backbone of the CPs with DPP core enables the use of shorter side chains because of the significant contribution of the furan rings to overall polymer solubility in common organic solvents. The PSCs based on furan-containing DPP copolymers and $PC_{71}BM$ showed PCE of 5.0%. Subsequently Fréchet group used long linear alkyl side chains as alternatives to branched side chains on furan-containing DPP copolymers to promote nanostructural order in thin-film solar cells and obtained the PCE of 6.5%.[24] These findings suggest the potential of furan moieties in the design of polymer donors for efficient organic photovoltaic applications. However generating suitable thin film morphologies of DPP copolymer:$PC_{71}BM$ blend requires the use of an additive or a solvent mixture in order to obtain high performance PSCs.[20, 24, 26, 27]

In this contribution, we present a furan-flanked DPP copolymer, poly{3,6-difuran-2-yl-2,5-di(2-octyldodecyl)-pyrrolo[3,4-c]pyrrole-1,4-dione-altthienylenevinylene} (PDVF-8) and highlight improving the PCE of the PSCs based on the PDVF-8 as an electron donor via solvent additive and methanol treatment (MT). Fig. 1 shows chemical structures of PDVF-8, device configuration of the PSCs based on PDVF-8 and $PC_{71}BM$ and energy level alignment of the materials used in the PSCs. Yu et al has reported that the PDVF-8 thin film has strong dual-band absorptions at 784 nm accompanied by a shoulder peak at 724 nm.[33] HOMO level versus vacuum level of the PDVF-8 thin film is 5.34 eV obtained from cyclic voltammetry.[33] Similar to many high-performance donor polymers, the PDVF-8 thin film mainly takes face-on orientation related to substrates because the (100) and (010) peaks could be clearly found in grazing incident x-ray scattering out-of- plane patterns with π–π stacking distances of 3.95 Å.[33] These properties imply that the PDVF-8 is a promising polymer donor for efficient PSCs. An ideal morphology for high performance photovoltaic devices requires nanoscale phase separation with a bicontinuous interpenetrating network, which can not only provide a large interface area between electron donor and acceptor materials for efficient exciton dissociation but also offer continuous pathways for more direct and quick charge transportation to the

[a]State Key Laboratory of Supramolecular Structure and Materials, Institute of Theoretical Chemistry, Jilin University, Changchun 130012, P. R. China. *E-mail: fhli@jlu.edu.cn (F. H. Li).
[b]Beijing National Laboratory for Molecular Sciences, Institute of Chemistry, Chinese Academy of Sciences, Beijing 100190, P. R. China. *E-mail: zhangwf@iccas.ac.cn (W. F. Zhang); yugui@iccas.ac.cn (G. Yu).
+Electronic Supplementary Information (ESI) available: [details of any supplementary information available should be included here]. See

corresponding electrodes so as to reduce charge recombination within the photoactive layer. Herein we investigated the effect of solvent additives (1, 8-diiodooctane (DIO) and 1-chloronaphthalene (CN)) and methanol treatment (MT) on the phase separation of the PDVF-8:PC71BM thin film using atomic force microscopy (AFM), transmission electron microscopy (TEM), TEM-energy dispersive spectroscopy (TEM-EDS) and x-ray photoemission spectroscopy (XPS) depth profiling in details.

2. Experimental details

2.1 Sample preparation

Synthesis of PDVF-8 can be found in Ref.33. $PC_{71}BM$ was purchased from American Dye Source, Inc (USA). To prepare PDVF-8:$PC_{71}BM$ (1:3, weight ratio) blend, the PDVF-8 and $PC_{71}BM$ were dissolved in three solvent systems (i) CF, (ii) CF with a small amount of DIO (1, 3 and 5 vol%, respectively) and (iii) CF with a small amount of CN (1, 3 and 5 vol%, respectively).

2.2 Device fabrication

ITO-patterned glass substrates were consecutively cleaned with acetone and ethanol in an ultrasonic bath. Surface of the glass substrates was modified by UV–ozone treatment for 20 minutes. A 35 nm thick PEDOT:PSS (Baytron PVP Al 4083) layer was spin-coated onto the cleaned ITO-patterned glass substrates, followed by annealing in air at 110 °C for 30 minutes under ambient condition. PDVF-8:$PC_{71}BM$ blend solutions were spin-coated on the surface of PEDOT:PSS layer to form a 100 nm thick film in the nitrogen-filled glove box. Then top surfaces of the blend films were treated by spin-coating methanol at 2000 rpm as illustrated in Fig. 1d. Finally, LiF (0.6 nm) and Al (100nm) were successively deposited by thermal evaporation under high vacuum (1×10^{-4} pa) onto the surface of the active layer. All devices have an active area of 2.0×2.0 mm^2.

2.3 Measurements and characterizations

Current density–voltage (J–V) characteristics of the devices were measured under N_2 atmosphere in the glove box by using Keithley 2400 under illumination and in the dark. Solar cell performance was tested under 1 sun, AM 1.5G full spectrum solar simulator (Photo Emission Tech. Inc., model #SS50AAA–GB) with an irradiation intensity of 100 mW cm^{-2} calibrated with a standard silicon photovoltaic traced to the National institute of metrology, China. Space charge limited current (SCLC) measurements were explored in device configurations of a) ITO/PEDOT:PSS/PDVF-8:$PC_{71}BM$/MoO_x/Al for hole-only device and b) ITO/Al/LiF/PDVF-8:$PC_{71}BM$/LiF/Al for electron-only device. External quantum efficiency (EQE) spectra were measured using Q Test Station 2000 (Crowntech Inc. USA) at room temperature in air.

AFM images were measured with an S II Nanonaviprobe station 300 HV (Seiko, Japan) in taping mode. TEM images and TEM-EDS mapping images were measured using JEM-2100F (JEOL, Japan).

XPS experiments were carried out using a VG Scienta R3000 spectrometer in ultrahigh vacuum with a base pressure of 2×10^{-10} mbar. The measurement chamber is equipped with a monochromatic Al (Kα) X-ray source providing photons with 1486.6 eV. 70 nm PDVF-8:$PC_{71}BM$ film was etched using an ion source (ISE5, Omicron Nano Tech. GmbH). S2p and C1s XPS spectra were measured after every etching with a time gap of 4 min.

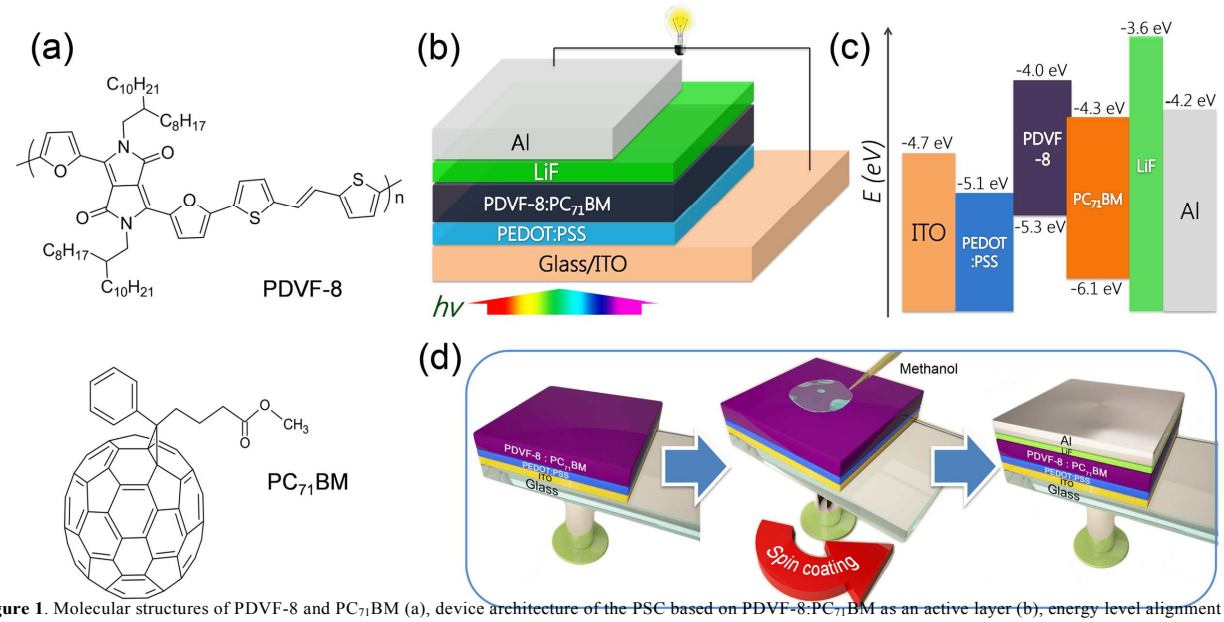

Figure 1. Molecular structures of PDVF-8 and $PC_{71}BM$ (a), device architecture of the PSC based on PDVF-8:$PC_{71}BM$ as an active layer (b), energy level alignment the materials used in the PSC (c) and schematic procedure for methanol treatment (d).

3. Results and discussion

In order to highlight the effect of solvent additives on the performance of the PSCs as shown in Fig 1b, the PDVF-8:$PC_{71}BM$ (1:3) thin film was spin-coated from CF, CF+3%DIO or CF+3%CN solution, respectively. We named the above 3 devices from various solvent/ solvent mixture as Device 1, 3 and 5, respectively. To further investigate MT on the performance of the PSCs, the PDVF-8:$PC_{71}BM$ thin films from CF, CF+3%DIO and CF+3%CN were treated by methanol so that Device 2, 4 and 6 were obtained. Fig. 2a presents current density versus voltage (J–V) characteristics of the above six PSCs under AM 1.5G illumination at 100 mW cm^{-2}. Open circuit (Voc), short circuit (Jsc), fill factor (FF), power conversion efficiency (PCE), series resistance (Rs) and shunt resistance (Rsh) derived from Fig. 2a are summarized in Table 1. It's apparent that photovoltaic performance of Device 1 is bad due to CF was used as a solvent of the active layer. The PCE of Device 2 is still below 1% because MT only slightly improved Jsc, Voc and FF. However when a small number of DIO or CN was added into CF solution of the PDVF-8:$PC_{71}BM$, the performance of the PSCs was greatly enhanced as shown in Fig. 2a. Three concentrations (1vol%, 3vol% and 5vol%) of DIO or CN have been tried in the solvent mixture with CF (Fig S1 and S2). Results demonstrated that even 1vol% DIO could give rise to an increase of PCE from 0.79% to 3.17% (Table S1). Addition of 3vol% and 5vol% DIO could improve the PCE to be 3.73% and 3.47%, respectively. Therefore 3vol% is regarded as an optimized concentration of DIO. Similarly addition of 3vol% CN as an optimized concentration resulted in a PCE of 4.26% (Table S2). If the surface of PDVF-8:$PC_{71}BM$ film spin-coated from CF + 3vol% CN was further treated by methanol, the PCE of Device 6 can reach 4.69% as shown in Table1. Because only 3vol% DIO or 3vol% CN in CF is involved, we simplify CF solution with 3vol% DIO or 3vol% CN as CF+DIO or CF+CN in the following descriptions. In order to ensure the validity and repeatability of data, we measured at least 20 pixels (size = 2 × 2 mm^2) for each device configuration. The average PCE values of Device 1 – 6 are 0.73%, 0.89%, 3.69%, 3.91%, 4.18% and 4.59%, respectively. Table 1 also presents series resistances (R_s) and shunt resistances (R_{sh}) of devices obtained from the slops of J-V curves at V_{OC} and J_{SC}, respectively (Fig. 2a). Compared to only-CF devices (Device 1 and 2), a decrease of R_s and an increase of R_{sh} are apparent when an additive (DIO or CN) was utilized in the solution of active layer. MT can further change the resistances. J_{sc} and FF increases of the devices (Device 3-6) with an additive (DIO or CN) are attributed to the resistance changes. In addition, the electrical leakage for the devices with an additive is suppressed because the Devices 3-6 have higher rectification ratios at ±1 V than the only-CF devices (Fig. S3). It indicates that solvent additives and/or MT can improve the diode quality and FF value. In order to detect a discrepancy of Jsc which easily leads to overvalued PCE,[34] external quantum efficiency (EQE) spectra of the Devices 1-6 from 300 nm to 900 nm were measured and shown in Fig. 2b. Jsc values calculated from integration of the EQE spectra of Device 1-6 are 2.69, 2.93, 9.05, 9.82, 10.35 and 11.05 mA cm^{-2}, respectively, which closely match Jsc = 2.9 mA cm^{-2} of Device 1 (ca. 7.2% error), Jsc = 3.1 mA cm^{-2} of Device 2 (ca. 5.5% error), Jsc = 9.73 mA cm^{-2} of Device 3 (ca. 7.0% error), Jsc = 10.3 mA cm^{-2} of Device 4 (ca. 4.7% error), Jsc = 10.89 mA cm^{-2} of Device 5 (ca. 5.0% error) and Jsc = 11.64 mA cm^{-2} of Device 6 (ca. 5.1% error) obtained from *J–V* characteristics under illumination. It means that the Jsc values measured for the PSCs are reliable and PCE values presented in this manuscript are not overvalued.

Compared to the only-CF devices, the devices with DIO or CN show higher FF values as listed in Table 1. It implies that the solvent additive effectively improved charge transport ability. In order to confirm the solvent additive and MT not only enhance electron and hole transport but also facilitate a balance of electron and hole transport in the PSCs, mobilities of electron and hole were measured in the electron-only and hole-only devices using space charge limited current (SCLC) method (details and parameters in Fig. S4a and b). The mobilities of electron and hole measured by SCLC are also listed in Table 1. The mobilities of electron and hole in the CF devices are 2.72×10^{-4} and 1.2×10^{-5} cm^2 V^{-1} s^{-1}, respectively. When the solvent additives were used, electron mobilities were slightly increased while hole mobilities were increased one order of magnitude. As a result, hole mobilities in CF+DIO and CF+CN devices are 8.89×10^{-5} and 1.15×10^{-4} cm^2 V^{-1} s^{-1}, respectively. It is worth noting that MT further increased the mobilities of electron and hole in all the devices. More importantly a perfect mobility balance of hole and electron has been achieved in the CF+DIO and CF+CN devices treated by methanol.

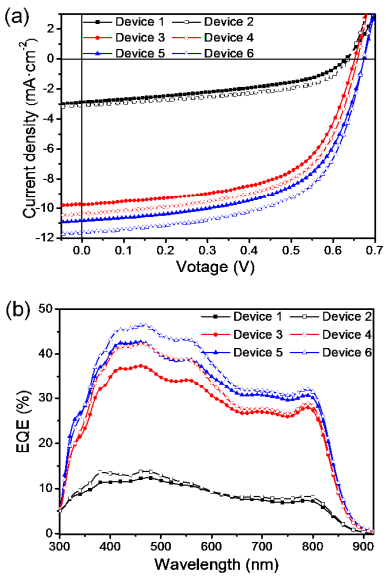

Figure 2. Current density versus voltage (J–V) characteristics of Device 1-6 under 100 mW cm^{-2} AM 1.5G illumination (a), EQE spectra of Device 1-6 (b). Device 1, 3 and 5 were spin-coated from CF (black solid squares), CF+DIO (red solid circles), CF+CN (blue solid triangles), respectively. Device 2, 4 and 6 were based on the active layer from CF treated by methanol (black hollow squares), CF+DIO treated by methanol (red hollow circles) and CF+CN treated by methanol (blue hollow triangles), respectively.

Table 1 Performances of PDVF-8:$PC_{71}BM$ PSCs from various solvent additive and methanol treatment

Device[a]	*Jsc* [mA cm^{-2}]	*Jsc-EQE* [mA cm^{-2}]	*Voc* [V]	FF [%]	PCE [%]		*Rs* [Ω cm^2]	*Rsh* [Ω cm^2]	Rectification Ratio	μ_e[b] [cm^2 V^{-1} s^{-1}]	μ_h[b] [cm^2 V^{-1} s^{-1}]
					Max.	Aver.					
1	2.90	2.69	0.630	0.432	0.79	0.73	53.6	528.4	1.6×10^{1}	2.72×10^{-4}	1.20×10^{-5}
2	3.10	2.93	0.635	0.495	0.98	0.89	32.6	692.4	4.4×10^{1}	3.00×10^{-4}	2.18×10^{-5}
3	9.73	9.05	0.650	0.590	3.73	3.69	7.2	910.6	4.0×10^{2}	3.76×10^{-4}	8.97×10^{-5}
4	10.30	9.82	0.655	0.597	4.03	3.91	7.0	956.1	6.0×10^{2}	3.84×10^{-4}	3.33×10^{-4}
5	10.89	10.35	0.670	0.583	4.26	4.18	7.7	868.7	1.2×10^{3}	4.34×10^{-4}	1.15×10^{-4}
6	11.64	11.05	0.670	0.601	4.69	4.59	6.2	1083.5	2.2×10^{3}	4.61×10^{-4}	4.54×10^{-4}

[a]Device structure: [ITO/PEDOT:PSS/PDVF-8:$PC_{71}BM$/LiF/Al]; PDVF-8:$PC_{71}BM$ layer of Device 1,3,5 with the active layer spin-coated from CF, CF+DIO, CF+CN respectively; Device 2, 4, 6 with the active layer from CF with MT, CF+DIO with MT, CF+CN with MT. [b]Charge carrier mobilities were obtained from electron-only and hole-only devices using SCLC method.

The enhanced Jsc and higher FF in the CF+DIO or CF+CN devices imply the formation of well-connected percolated networks for each of the phase-separated components (donor and acceptor). To gain an insight for the relation between phase separation in the PDVF-8:$PC_{71}BM$ blend film and device performance, morphologies of the PDVF-8:$PC_{71}BM$ films spin-coated from CF, CF+DIO and CF+CN have been investigated using AFM and TEM. Fig. 3 shows the surface morphologies obtained by AFM measured at ambient, where a1-f1 for height images and a2-f2 for phase images. The surfaces of PDVF-8:$PC_{71}BM$ films from CF are quite rough due to a root- mean-square (RMS) roughness of 12.6 nm for the film without MT (Fig. 3a) and a roughness of 11.62 nm for the film with MT (Fig. 5b). Both Fig. 3a and 3b exhibit coarse cobblestone-like phase separation with large microscale domains which are consistent with observations in other DPP-polymers:$PC_{71}BM$ blend films from only CF[35, 36] and chlorobenzene (CB)[20]. However the surfaces of PDVF-8:$PC_{71}BM$ films spin-coated from CF+DIO or CF+CN become much smoother and more homogeneous as shown in Fig. 3c-f. Apparently aggregations were significantly suppressed by adding DIO or CN into CF. The surface roughness of PDVF-8:$PC_{71}BM$ film from CF+DIO is 1.28 nm in Fig. 3c. When the surface of the PDVF-8:$PC_{71}BM$ film from CF+DIO is treated by methanol, the RMS roughness become 1.03 nm in Fig. d. When using CF+CN as a solvent, the surface roughness of PDVF-8:$PC_{71}BM$ film without MT decrease to 0.9 nm (Fig. 3e) and the surface roughness of PDVF-8:$PC_{71}BM$ film with MT further decrease to 0.87 nm (Fig. 3f). The reduced surface roughness implies that PDVF-8 and $PC_{71}BM$ were better mixed. Therefore both DIO and CN as a solvent additive led to an obvious reconstruction of the surface morphologies of the PDVF-8:$PC_{71}BM$ blends from microscale to nanoscale. Effects of solvent additive and MT on bulk morphologies of PDVF-8:$PC_{71}BM$ blends have been studied by TEM imaging as well. Fig. 4 demonstrates the TEM images of PDVF-8:$PC_{71}BM$ films spin-coated from CF, CF+DIO and CF+CN with (a, c and e) and without (b, d and f) MT. Large dark clusters (300-500 nm) are observed in the CF films shown in Fig. 4a and b which are consistent with the AFM images in Fig. 3a and b. The higher electron density of $PC_{71}BM$ compared with the polymer causes electrons to be scattered more efficiently by the $PC_{71}BM$ from the TEM beam. Thus, the darker regions in the TEM images are regions of phase-separated $PC_{71}BM$. Because the exciton diffusion length (<10 nm) is much smaller than the 300–500 nm clusters as seen in Fig. 4a and b, photo-generated excitons will often decay before reaching the interfaces between PDVF-8 and $PC_{71}BM$ in the films spin-coated from CF, resulting in a concomitant loss of photocurrent in Fig. 2a. However DIO as an additive results in significantly smaller nanoscale phase separation in Fig. 4c and d. CN replacing DIO can make the nanoscale phase separation further finer in Fig. 4e and f. Moreover fibrillar PDVF-8 nanostructures are pronounced in Fig. 4c-f. Thus using DIO or CN leads to not only smaller nanoscale phase separation but also better-connected percolated networks, causing the PDVF-8 network to form longer and better connected pathways. The morphology change can correspond to the great increase of hole mobility as shown in Table 1.

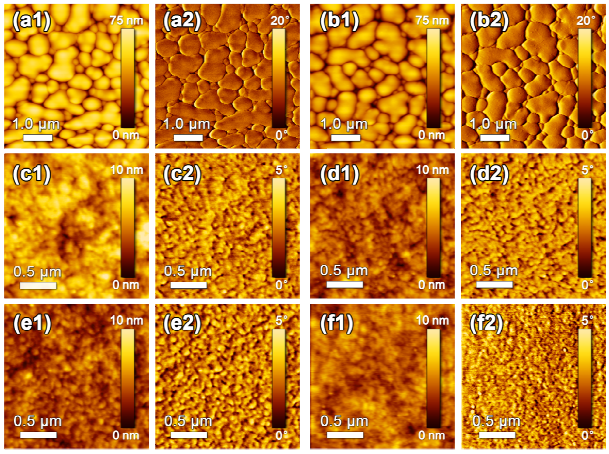

Figure 3. AFM height and phase images of PDVF-8:$PC_{71}BM$ film spin-coated from CF without (a) and with (b) methanol treatment, from CF+DIO without (c) and with (d) methanol treatment, from CF+ N without (e) and with (f) methanol treatment. a1-f1 for height images and a2-f2 for phase images.

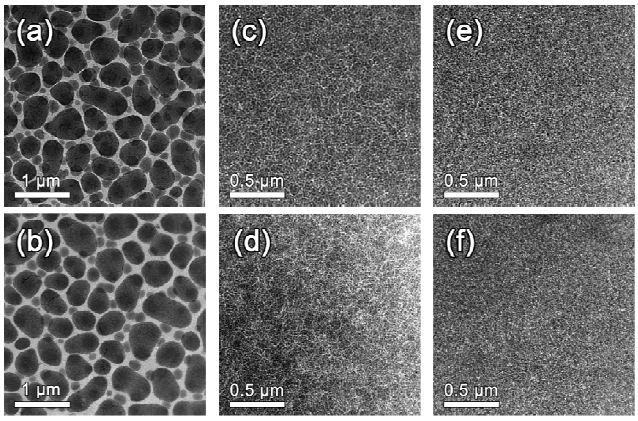

Figure 4. TEM images of PDVF-8:$PC_{71}BM$ film spin-coated from CF without (a) and with (b) methanol treatment, from CF+DIO without (c) and with (d) methanol treatment, from CF+CN without (e) and with (f) methanol treatment.

Herein we try to provide a reasonable explanation for the morphology changes of PDVF-8:$PC_{71}BM$ film from microscale to nanoscale by using small amounts of an additive (DIO or CN) as follows. Both DIO and CN are bad solvent for PDVF-8. In our experiments, we found that PDVF-8 solubility in CN was lower than 1.5 mg/ml and PDVF-8 solubility in DIO was even lower than in CN. However $PC_{71}BM$ solubility in both DIO and CN is greater than 400 mg/ml. It seems that both DIO and CN have a similar working mechanism for the film morphology of PDVF-8:$PC_{71}BM$ from the CF+DIO or CF+CN. During spin-coating the PDVF-8:$PC_{71}BM$ from CF with a low boiling point (61 °C), the intermolecular stacking of PDVF-8 and aggregation of $PC_{71}BM$ more easily and rapidly occur due to quite fast evaporation of CF. Namely some portion of $PC_{71}BM$ would be situated between PDVF-8 chains to form some big size domains (300-500 nm) which hindered the formation of bicontinuous interpenetrating networks in the active layer. However high boiling point additive (332 °C for DIO and 260 °C for CN) gave rise to a change in the kinetics of film growth. DIO or CN, with a high boiling point and a high $PC_{71}BM$ solubility can prolong the solvent evaporation time to provide enough time for the complete film formation and dissolve many $PC_{71}BM$ molecules even in the bimolecular structure. This process prevented the formation of bimolecular structure and facilitated better nanoscale phase separation of PDVF-8 and $PC_{71}BM$, leading to the bicontinuous change carrier pathway with an enlarged interfacial area.[37]

In order to further prove that introduction of a little additive suppressed the aggregation of $PC_{71}BM$ and gave rise to better connected pathways of PDVF-8 and a bicontinuous interpenetrating network of PDVF-8 and $PC_{71}BM$, we detected distributions of sulphur (S) and carbon (C) elements of PDVF-8:$PC_{71}BM$ film using TEM-energy dispersive spectrum (TEM-EDS) mapping in a smaller size. Because only PDVF-8 includes S atoms, S can be regarded as a sign of the polymer in the images. For comparison, S and C distributions on the PDVF-8:$PC_{71}BM$ film from CF, CF+CN and CF+CN with MT were mapped by the SEM-EDS in Fig. 5, where yellow dots are sulfur element (b, e, h) and white dots are carbon element (c, f, i). At the same time, TEM images in smaller size than Fig. 4 are also presented in Fig. 5a, d and g. For the film from CF, enriched C regions in the 4 corners of Fig. 5c correspond to dark regions of $PC_{71}BM$ in Fig. 5a and enriched S regions in Fig. 5b correspond to light region of PDVF-8 in Fig. 5a. Obviously both PDVF-8 and $PC_{71}BM$ have a poor discrete phase separation in the film from CF. However, distributions of S (Fig. 5e) and C (Fig. 5f) become homogeneous for the film from CF+CN. Therefore both PDVF-8 and $PC_{71}BM$ have a continuous phase separation which facilitates the transport of charge carriers, in particular hole in the PDVF-8:$PC_{71}BM$ (1:3) blend film from CF+CN. At the same time interfacial areas between PDVF-8 and $PC_{71}BM$ are greatly improved because their phase separation changed from microscale into nanoscale as shown in Fig. 5d. Furthermore MT can lead to denser and more uniform dots of S in Fig. 5h and C in Fig. 5i, resulting in finer phase separation in Fig. 5g than the film without MT in Fig. 5d. As a result, MT which further polished nonoscale phase separation of PDVF-8 and $PC_{71}BM$ gave rise to more enhancements in mobilities of electron and hole as shown in Table1.

In addition, EQE spectra in Fig. 2b have presented some interesting information. For a given wavelength, the EQE values increase in the order CF < CF+DIO < CF+CN, which is consistent with the Jsc values from J–V curves under illumination. For all devices, higher EQE values are observed at 300-650 nm which is in the absorption region of $PC_{71}BM$.[35] Because PDVF-8 hardly has an absorption in the short wavelength region, we assign EQE spectra at 300-650 nm to the contribution of $PC_{71}BM$ and EQE spectra at 650-900 nm to the contribution of PDVF-8. Compared to Device1 without MT, the EQE spectrum of Device 2 with MT has a slightly increase for all wavelengths at 300-900 nm. However for the devices with an additive (DIO or CN), MT only leads to a lift of the EQE spectra at 300-650 nm as shown in Fig. 2b. The EQE spectra at 650-900 nm of the devices (Device 4 or 6) with MT are not different from the devices without MT (Device 3 or 5). Because alcohol treatments do not change the light absorption of the components in the active layer blend[38] we infer that MT more efficiently improved separation and transport of excitons formed in $PC_{71}BM$ than one of the excitons in PDVF-8. Therefore the EQE changes caused by MT originate from the reconstructed morphologies of the active layer blend, in particular $PC_{71}BM$.

Besides the lateral phase separated morphology, the vertical distribution of the components in the blend film is also critical. To verify the proposed morphology evolution during the MT, we focus on investigating the effect of MT on the vertical phase separation of PDVF-8 and $PC_{71}BM$ in the blend from CF+CN employing XPS depth profiling. S2p peak represents PDVF-8. C1s peak represents the total content of PDVF-8 and $PC_{71}BM$. S2p/C1s peak area ratio could be proportionally correlated to the percentage of PDVF-8 in the blend. Therefore, PDVF-8 to $PC_{71}BM$ weight ratios in the vertical direction from top to bottom can be evaluated by using S/C peak area ratios in XPS depth profiling (Fig. S5). Fig. 6a presents S/C ratio versus etching time for 70 nm PDVF-8:$PC_{71}BM$ film from CF+CN. Because 17 nm can be removed in 4-minute etching, 0, 4, 8 and 12-minute etchings approximately correspond to 70 nm (top

surface), 53 nm, 36 nm and 19 nm (bottom) from bottom to top. For the pristine film without MT, S/C ratio at the top surface is nearly three times of one at the bottom, suggesting higher PDVF-8 concentration at the top surface and higher $PC_{71}BM$ concentration at the bottom. When the film was treated by spin-coating methanol, the S/C ratio of the top surface reduced nearly half of that of the pristine film while the S/C ratio of the bottom heightened nearly half of that of the pristine film. It indicates that PDVF-8 concentration at the top surface and $PC_{71}BM$ concentration at the bottom are decreased while PDVF-8 concentration at the bottom and $PC_{71}BM$ at the top surface are increased by MT. In addition, MT makes the PDVF-8 better-distributed in vertical direction because 4 red S/C ratios are close each other after MT. And concentration of PDVF-8 at the bottom is slightly higher than at the top surface after MT. Therefore a more uniform and homogeneous distribution was formed by MT in the vertical direction. In order to explain these findings, the detailed evolution of phase separation in the blend film is schematically illustrated in Fig. 6b. Polymers and small molecule $PC_{71}BM$ tend to aggregate on the top surface and bottom surface respectively during the spin-coating due to their different surface energies.[39 40] After methanol was spin-coated on the PDVF-8:$PC_{71}BM$ film, it quickly penetrated into the film. Because CN is a good solvent for $PC_{71}BM$ and bad solvent for PDVF-8, residual CN in the PDVF-8:$PC_{71}BM$ film can exist in the form of the solvent of $PC_{71}BM$. During the evaporation of methanol which is highly intersoluble with CN, $PC_{71}BM$ accompanying CN migrated and diffused from the bottom contacting with PEDOT:PSS to the top surface of the active layer, which is in agreement with the observations by Li et al. in the P3HT:$PC_{61}BM$ system[41] and by Zhao et al. in the PTB7-Th:$PC_{71}BM$ system.[42] As a result, vertical distributions of PDVF-8 and $PC_{71}BM$ become more uniform in the active layer of PSCs, which not only provide a large interface area between PDVF-8 and $PC_{71}BM$ for efficient exciton dissociation but also offer continuous pathways for more direct and quick charge transportation to the corresponding electrodes.

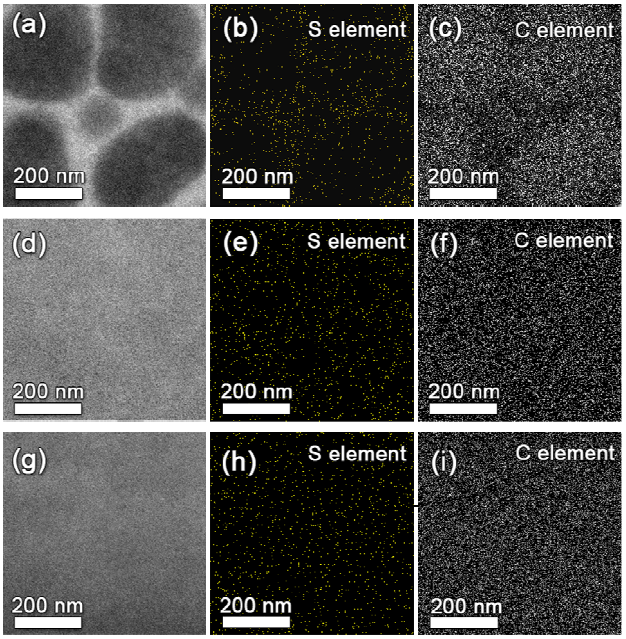

Figure 5. Transmission electron microscopy-energy dispersive spectroscopy (TEM-EDS) images of PDVF-8:$PC_{71}BM$ film spin-coated from CF (a-c), CF+CN without (d-f) and with (g-i) MT. The yellow dots (b, e, h) signify sulfur element; The white dots (c, f, i) signify carbon element; (a), (d) and (g) are TEM images

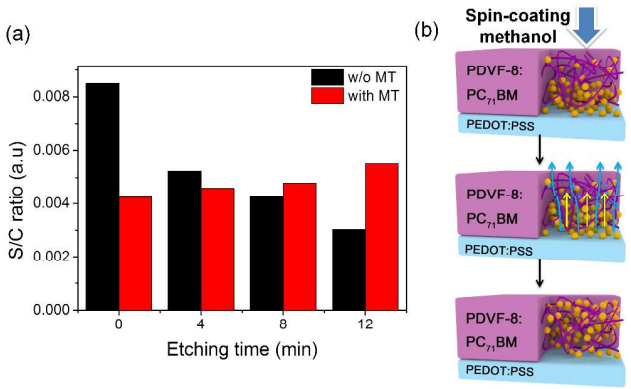

Figure 6. Vertical S/C ratio in PDVF-8:$PC_{71}BM$ film spin-coated from CF+CN without and with MT (a). Schematic illustration of the detailed morphology evolution in PDVF-8:$PC_{71}BM$ film after spin-coating methanol (b). Purple wires: PDVF-8 polymer chains; big orange dots: $PC_{71}BM$; blue dots: methanol.

4. Conclusion

Effects of solvent additives (DIO and CN) and MT on the device performance of the PSCs base on a furan-flanked DPP copolymer, PDVF-8 have been investigated. When 3vol% DIO or CN was used as a solvent additive of PDVF-8:$PC_{71}BM$ solution in CF, the PCE can increase from 0.79% to 3.73% or 4.26%. MT can further enhance the PCE to 4.03% (DIO) and 4.69% (CN), respectively. AFM images demonstrated that both DIO and CN led to an obvious reconstruction of the surface morphologies of the PDVF-8:$PC_{71}BM$ blends from microscale to nanoscale. TEM and TEM-EDS images showed that using DIO or CN gave rise to not only smaller nanoscale phase

separation but also better-connected percolated networks. XPS depth profiling proved that MT resulted in a more uniform vertical distributions of PDVF-8 and $PC_{71}BM$ in the blend because MT induced migration and diffusion of PCBM from the bottom contacting with PEDOT:PSS to the top surface of the active layer. The lateral and vertical nanoscale phase separations with a bicontinuous interpenetrating network induced by solvent additives and MT not only provided a large interface area between PDVF-8 and $PC_{71}BM$ for efficient exciton dissociation but also offered continuous pathways for more direct and quick charge transportation to the corresponding electrodes so as to reduce charge recombination within the photoactive layer.

Acknowledgements

This work was supported by grants from the National Basic Research Program of China (2014CB643505) and the Natural Science Foundation of China (51273077).

Notes and references

1 G. Yu, J. Gao, J. C. Hummelen, F. Wudl, A. J. Heeger, *Science,* 1995, **270**, 1789.
2 B. C. Thompson, J. M. J. Fréchet, *Angew. Chem., Int. Ed.,* 2008, **47**, 58.
3 Y. Li, *Accounts Chemical Research* 2012, **45**, 723.
4 G. Li, R. Zhu, Y. Yang, *Nat. Photonics,* 2012, **6**, 153.
5 Y. Liang, L. Yu, *Accounts Chemical Research,* 2010, **43**, 1227.
6 Z. C. He, C. Zhong, X. Huang, W.Y. Wong, H. Wu, L. Chen, S. Su, Y. Cao, *Adv. Mater.*, 2011, **23**, 4636.
7 Z. C. He, C.M. Zhong, S. J. Su, M. Xu, H. B. Wu, Y. Cao, *Nat. Photonics,* 2012, **6**, 591.
8 C. Gu, Y.C. Chen, Z.B. Zhang, S.F. Xue, S.H. Sun, K. Zhang, C.M. Zhong, H.H. Zhang, Y. Lv, F.H. Li, F. Huang, Y.G. Ma, *Advanced Energy Materials*, 2014, **4**, 1301771.
9 Y. Liu, J. Zhao, Z. Li, C. Mu, W. Ma, H. Hu, K. Jiang, H. Lin, H. Ade, H. Yan, *Nat. Commun*, 2014, **5,** 5293.
10 X. Cheng, S. H. Sun, Y. C. Chen, Y. J. Gao, L. Ai, T. Jia, F. H. Li, Y. Wang, *J. Mater. Chem. A*, 2014, **2**, 12484.
11 M. Scharber, D. Mühlbacher, M. Koppe, P. Denk, C. Waldauf, A. Heeger, C. Brabec, *Adv. Mater*, 2006, **18**, 789.
12 W. W. Li, K. H. Hendriks, A. Furlan, M. M. Wienk, R. A. J. Janssen, *J. Am. Chem. Soc*, 2015, **137**, 2231
13 B. C. Thompson, J. M. J. Fréchet, *Angew. Chem., Int. Ed*., 2008, **47**, 58.
14 R. A. J. Janssen, J. Nelson, *Adv. Mater.* 2013, **25**, 1847.
15 M. Jeffries-EL, B. M. Kobilka, B. J. Hale, *Macromolecules*, 2014, **47**, 7253.
16 P. M. Beaujuge, C. M. Amb, J. R. Reynolds, *Acc. Chem. Res.,* 2010, **43**, 1396.
17 S. Y. Qu, H. Tian, *Chem. Commun*., 2012, **48**, 3039.
18 M. M. Wienk, M. Turbiez, J. Gilot, R. A. J. Janssen, *Adv. Mater,*. 2008, **20**, 2556.
19 K. H. Hendriks, W. W. Li, M. M. Wienk, R. A. J. Janssen, *Adv. Energy Mater.,* 2013, **3**, 674.
20 C. H. Woo, P. M. Beaujuge, T. W. Holcombe, O. P. Lee, J. M. J. Fréchet, *J. Am. Chem. Soc.*, 2010, **132**, 15547.
21 J. C. Bijleveld, A. P. Zoombelt, S. G. J. Mathijssen, M. M. Wienk, M. Turbiez, D. M. de Leeuw, R. A. J. Janssen, *J. Am. Chem. Soc.*, 2009, **131**, 16616.
22 H. N. Tsao, D. M. Cho, I. Park, M. R. Hansen, A. Mavrinskiy, D. Y. Yoon, R. Graf, W. Pisula, H. W. Spiess, K. Mullen, *J. Am. Chem. Soc.*, 2011, **133**, 2605.
23 J. C. Bijleveld, B. P. Karsten, S. G. J. Mathijssen, M. M. Wienk, D. M. de Leeuw, R. A. J. Janssen, *J. Mater. Chem.*, 2011, **21**, 1600.
24 A. T. Yiu, P. M. Beaujuge, O. P. Lee, C. H. Woo, M. F. Toney, J. M. J. Fréchet, *J. Am. Chem. Soc.*, 2012, **134**, 2180.
25 L. T. Dou, J. Gao, E. Richard, J. B. You, C. –C. Chen, K. C. Cha, Y. J. He, G. Li, Y. Yang, *J. Am. Chem. Soc.*, 2012, **134**, 10071.
26 L. Ye , S. Q. Zhang , W. Ma , B. H. Fan , X. Guo , Y. Huang , H. Ade, J. H. Hou, *Adv. Mater*., 2012, **24**, 6335.
27 S. Q. Zhang, L. Ye, Q. Wang, Z. J. Li, X. Guo, L. J. Huo, H. L. Fan, J. H. Hou, *J. Phys. Chem. C*, 2013, **117**, 9550.
28 W. W. Li, K. H. Hendriks, A. Furlan, W. S. C. Roelofs, M. M. Wienk, R. A. J. Janssen, *J. Am. Chem. Soc.*, 2013, **135**, 18942.
29 L. Bürgi, M. Turbiez, R. Pfeiffer, F. Bienewald, H. J. Kirner, C. Winnewisser, *Adv. Mater.,* 2008, **20**, 2217 .
30 Z. Chen, M. J. Lee, R. Shahid Ashraf, Y. Gu, S. Albert-Seifried, M. Meedom Nielsen, B. Schroeder, T. D. Anthopoulos, M. Heeney, I. McCulloch, H. Sirringhaus, *Adv. Mater.,* 2012, **24**, 647.
31 H. Chen, Y. Guo, G. Yu, Y. Zhao, J. Zhang, D. Gao, H. Liu, Y. Liu, *Adv. Mater*., 2012, **24**, 4618.
32 C. B. Nielsen, M. Turbiez, I. McCulloch, *Adv. Mater.,* 2013, **25**, 1859.
33 H. J. Chen, Y. L. Guo, Z. P. Mao, D. Gao, G. Yu, *J. Polym. Sci. Part A: Polym. Chem.,* 2014, **52**, 1970.
34 E. Zimmermann, P. Ehrenreich, T. Pfadler, J. A. Dorman, J. Weickert, L. Schmidt-Mende, *Nat. Photonics,* 2014, **8**, 669.
35 S. K. Son, H. –S. Lee, J. S. Ha, K. H. Kim, H. J. Son, M. J. Ko, H. Kim, D. –K. Lee, J. Y. Kim, W. Lee, S. Park, D. H. Choi, B. Kim, *Sol. Energy Mater. Sol. Cells*, 2014, **124**, 232.
36 E. L. Williams, S. Gorelik, I. Y. Phang, M. Bosman, C. Vijila, G. S. Subramanian, P. Sonar, J. Hobley, S. P. Singh, H. Matsuzaki, A. Furube, R. Katoh, RS*C Adv.*, 2013, **3**, 20113.
37 S. Kwon, J. K. Park, J. Kim, G. Kim, K. Yu, J. Lee, Y. R. Jo, B. J. Kim, H. K. Kang, J. W. Kim, H. Kim, K. H. Lee, *J. Mater. Chem. A*, 2015, **3**, 7719.
38 S. Guo, B. Cao, W. J. Wang, J. –F. Moulin, P. Müller-Buschbaum, *ACS Appl. Mater. Interfaces*, 2015, **7**, 4641.
39 M. Campoy-Quiles, T. Ferenczi, T. Agostinelli, P. G. Etchegoin, Y. Kim, T. D. Anthopoulos, P. N. Stavrinou, D. D. C. Bradley, J. Nelson, *Nat. Mater.,* 2008, **7**, 158.
40 Z. Xu, L. M. Chen, G. W. Yang, C. H. Huang, J. H. Hou, Y. Wu, G. Li, C. S. Hsu, Y. Yang, *Adv. Funct. Mater.,* 2009, **19**, 1227.
41 H. Li, H. W. Tang, L. G. Li, W. T. Xu, X. L. Zhao, X. N. Yang, *J. Mater. Chem..,* 2011, **21**, 6563.
42 L. Zhao, S. L. Zhao, Z. Xu, Q. Q. Yang, D. Huang, X. R. Xu, *Nanoscale*, 2015, **7**, 5537.